Oscillatory bubbles induced by geometrical constraint

M. Pailha, A. L. Hazel, P. A. Glendinning, and A. Juel

Citation: Phys. Fluids **24**, 021702 (2012); doi: 10.1063/1.3682772
View online: http://dx.doi.org/10.1063/1.3682772
View Table of Contents: http://pof.aip.org/resource/1/PHFLE6/v24/i2
Published by the American Institute of Physics.

Oscillatory bubbles induced by geometrical constraint

M. Pailha,[a] A. L. Hazel, P. A. Glendinning, and A. Juel[b]
Manchester Centre for Nonlinear Dynamics and School of Mathematics, University of Manchester, Oxford Road, Manchester M13 9PL, United Kingdom

(Received 29 September 2011; accepted 3 January 2012; published online 9 February 2012)

We show that a simple change in pore geometry can radically alter the behavior of a fluid-displacing air finger, indicating that models based on idealized pore geometries fail to capture key features of complex practical flows. In particular, partial occlusion of a rectangular cross section can force a transition from a steadily propagating centered finger to a state that exhibits spatial oscillations formed by periodic sideways motion of the interface at a fixed distance behind the moving finger tip. We characterize the dynamics of the oscillations, which suggest that they arise from a global homoclinic connection between the stable and unstable manifolds of a steady, symmetry-broken solution. © *2012 American Institute of Physics*. [doi:10.1063/1.3682772]

The displacement of one fluid by another underpins many physical processes of considerable economic and medical significance, including oil extraction from porous media,[1] emerging lab-on-a-chip technologies,[2] and the biomechanics of the lungs.[3] In idealized pore geometries, where cross sections are characterized by a single length scale, i.e., circular, rectangular, or polygonal,[4–7] a unique family of steadily propagating centered fingers develops when air is driven through a pore initially filled with a viscous liquid. These fingers are surrounded by a film of the liquid whose thickness increases monotonically with the capillary number, $Ca = \mu U/\sigma$, the ratio of viscous to surface-tension forces: μ is the viscosity difference between the two fluids, U is the velocity of the finger tip, and σ is the interfacial tension.

In this contribution, we show that a simple change in cross-sectional geometry can dramatically alter the dynamics, inducing spontaneous periodic deformations of the finger as it advances along an axially uniform rectangular tube in which the depth of the cross section is locally reduced by a centered rectangular occlusion, see Fig. 1. After the passage of the finger, which continues to advance at a constant speed (with a maximum variability of less than 2%), the interface rapidly approaches a state of quasi-static equilibrium and the periodic deformations form a spatially periodic pattern that remains fixed in the laboratory frame. The existence of these novel propagation modes suggests that models based on over-simplification of the pore geometry will suppress fundamental physical behavior present in practical applications, where pore geometry often contains many regions of local constriction, e.g., connecting or irregularly shaped pores in carbonate oil reservoirs,[8] and airway collapse or mucus buildup in the lungs.[9] Moreover, these modes offer further potential for geometry-induced manipulation of droplets for lab-on-the-chip applications, in which geometric variations have so far been restricted to the axial direction.[10–12]

The spatially periodic pattern is "shed" by the steadily advancing finger, which exhibits local oscillatory sideways motion of its interface behind the tip. The amplitude of the oscillation increases beyond L_{tip}, defined as the distance behind the finger tip where the finger first spreads laterally over the entire obstacle. The periodic deformation of the finger tip is shown in Fig. 2, where snapshots of the tip are presented for successive times over one period of oscillation. We also show the form of the

[a] Also at LOCIE, CNRS UMR 5271, Université de Savoie, Campus Scientifique, Savoie Technolac, 73376 Le Bourget du Lac Cedex, France.
[b] Electronic mail: anne.juel@manchester.ac.uk.

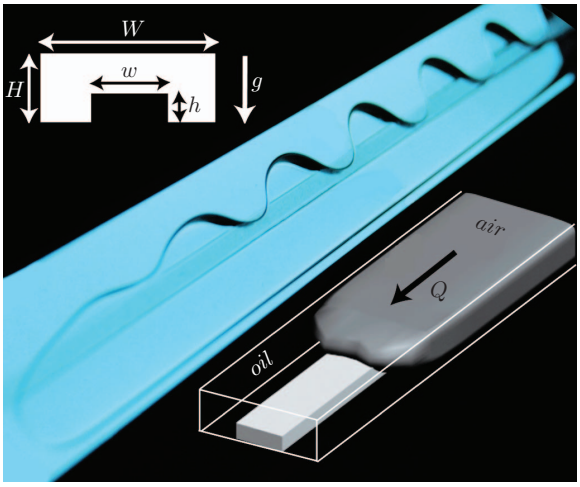

FIG. 1. (Color online) Spontaneous periodic oscillations develop along an air finger that displaces oil from a axially uniform tube with a partially occluded rectangular cross section, when driven at a constant flow rate Q (see schematic diagram in bottom-right corner). Once fully developed, the oscillations remain fixed in the lab frame. The tube is horizontal in the experiments as indicated in the cross section shown in the top-left corner, and the apparent tilt of the tube in the photograph is due to the angle of view of the camera. The ratio of obstacle width to tube width is $\alpha_w = w/W = 1/7$; the height ratio is $\alpha_h = h/H = 0.35$; and gravity acts normal to the direction of propagation. The dimensionless speed of the finger tip is $Ca = \mu U/\sigma = 0.5$.

sideways oscillation of a point on the edge of the finger at a fixed distance (33 mm) behind the tip, chosen in the region where the finger deformation is significant (see supplementary material[19] for movies of the temporal development of the spatially periodic pattern). Hence, the pattern does not form uniformly along the interface, in contrast to surface-tension-driven breakup (Rayleigh–Plateau) and gravity-induced dripping (Rayleigh–Taylor) instabilities.[13] Fundamental changes in the nature of air-finger propagation within the tube were demonstrated in a similar occluded geometry,[14] via the realization of steadily propagating, asymmetric fingers that localize in the least-constricted regions of the cross section. These asymmetric fingers were found to limit the amount of liquid recovered

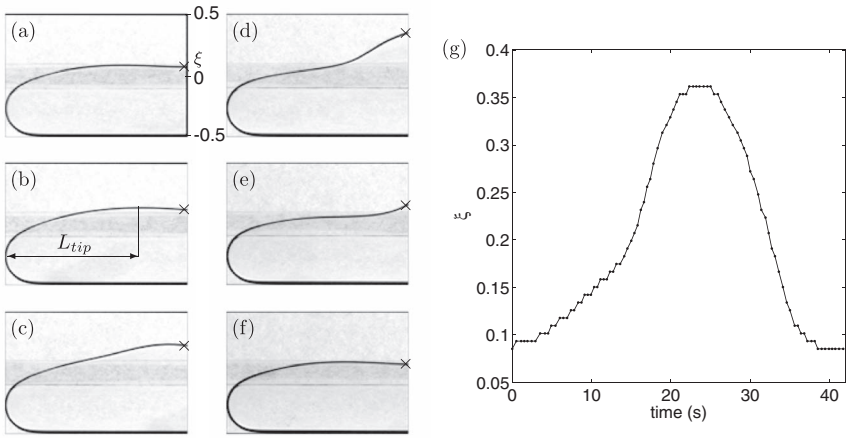

FIG. 2. Finger tip evolution during one cycle of oscillation of period $\tau = 41.7$ s for $\alpha_w = 1/5$, $\alpha_h = 0.35$, and $Ca = 1.59 \times 10^{-2}$: (a) $t = 0$, (b) $t = 0.19\tau$, (c) $t = 0.40\tau$, (d) $t = 0.60\tau$, (e) $t = 0.81\tau$, (f) $t = \tau$. The length of the tip L_{tip} is defined as the distance behind the tip at which the finger first passes laterally over the entire obstacle. Each finger is moving from right to left. The length of the side of each pixel in the photographs corresponds to 1.8×10^{-1} mm. (g) Time evolution of ξ, the distance of the edge of the interface from the centreline of the tube divided by the tube width, at a fixed distance, 33 mm, behind the finger tip. The edge of the obstacle corresponds to $\xi = 0.1$ and the tube wall is located at $\xi = 0.5$.

from the tube as quantified by the wet fraction, m: the ratio of the liquid volume extracted to the total volume of a fixed length of tube. The finger shown in Fig. 1 oscillates periodically between near-symmetric and localized configurations, indicating that in this regime both states coexist and are weakly unstable. Based on detailed experimental observations, we propose a consistent bifurcation scenario, which suggests that the origin of the oscillations is a global homoclinic bifurcation.

We conducted a series of experiments in rectangular tubes formed of stainless steel strips separating two horizontal float-glass sheets, each containing a rigid rectangular Perspex rod of width $w = 4.49 \pm 0.01$ mm positioned symmetrically halfway across the bottom boundary of the tube (see Fig. 1). The height of the tubes was fixed at $H = 3.07 \pm 0.01$ mm, sufficiently large to allow the introduction of two different occlusion heights, $h = 1.09 \pm 0.01$ and 1.50 ± 0.02 mm, giving two obstacle height ratios of $\alpha_h = h/H = 0.35$ and 0.49. As noted in Ref. 15, a millimetric tube height enabled accurate control of α_h, but also meant that gravitational effects could not be neglected: the ratio of typical hydrostatic to capillary pressure differences is quantified by the Bond number $Bo = \rho g b^2/4\sigma \approx 1.0$ (ρ is the density of the liquid and g is the acceleration due to gravity). The tube width was varied to yield tube aspect ratios in the range $2.56 \leq \alpha = W/H \leq 10.24$, which are typical of microfluidic channels, and also obstacle width ratios in the range $1/7 < \alpha_w = w/W < 4/7$. The tubes were uniform to better than 0.3% and 0.8% of their heights and widths, respectively.[15] The occlusions were machined from Perspex to enable direct visualization and were bonded to the bottom glass plate of the tube to yield a 50 cm long axially uniform, constricted tube. The errors in the positional accuracy and axial uniformity of the occlusions were better than 0.5% and 3% of the occlusion width, respectively.

Initially, each tube was completely filled with silicone oil (Basildon Chemicals Ltd., $\mu = 5.4 \times 10^{-2}$ Pa s and $\sigma = 2.1 \times 10^{-2}$ N m^{-1}). A two-phase displacement flow was induced by withdrawing liquid at a constant volumetric flow rate using a syringe pump connected to one end of the tube; the other end remained open to the atmosphere. A short inlet section of rectangular cross section ensured that the finger was initially centered and symmetric about the mid-plane of the tube. The system rapidly adjusted to a new state after entering the occluded tube, and transients decayed over very short distances for all flow rates away from critical points. The motion of the steadily propagating finger tip was recorded with a top-view megapixel camera over a distance of 20 cm towards the end of the tube, and the velocity of the finger tip, and hence the capillary number, was determined from image analysis of the frames. Overview photos were also taken to characterize the spatially periodic bubbles with a high resolution (3872 × 2592 pixel) still camera.

Top views of the air finger are shown in Figs. 3(a)–3(e) for increasing capillary number (or flow rate) when $\alpha_h = 0.49$ and $\alpha_w = 1/3$. At low Ca, Fig. 3(a), the finger remains approximately symmetric with no axial periodicity. Over a wide range of intermediate capillary numbers, Figs. 3(b)–3(d), temporal oscillations of the interface at a fixed distance behind the moving tip lead to the "shedding" of a regular pattern with a Ca-dependent spatial period. Once fully developed, the "shed" pattern remains fixed in the lab frame, but in a frame moving with the constant velocity of the finger tip the oscillations will first appear at a fixed spatial location and then increase in amplitude as they are advected away from the tip at constant speed. At the highest Ca shown, Fig. 3(e), the oscillations cease and the air finger is uniformly asymmetric after the initial transition

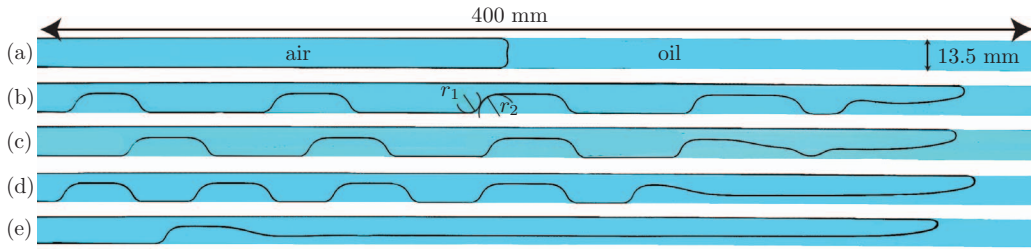

FIG. 3. (Color online) Top view snapshots of air fingers advancing steadily from left to right in a rectangular tube containing a high obstacle ($\alpha_h = 0.49$ and $\alpha_w = 1/3$) for capillary numbers (a) $Ca = 3.46 \times 10^{-3}$, (b) $Ca = 5.74 \times 10^{-3}$, (c) $Ca = 7.14 \times 10^{-3}$, (d) $Ca = 1.40 \times 10^{-2}$, and (e) $Ca = 2.48 \times 10^{-2}$.

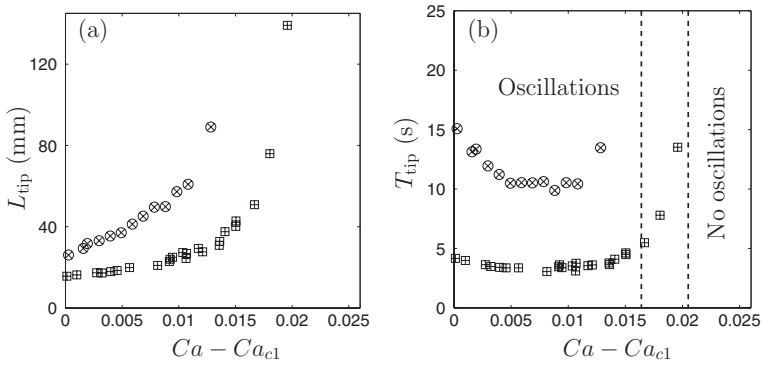

FIG. 4. (a) Characteristic tip length ($L_{\rm tip}$), the distance from the tip to the position at which the rapid sideways movement associated with the finger passing over the obstacle first occurs, $x_{\rm tip}$, plotted as a function of difference from the capillary number at which the oscillations begin, Ca_{c1}. (b) Characteristic time scale ($T_{\rm tip}$), the difference between the times when the first oscillation develops and when the tip is at $x_{\rm tip}$. The data are for a high obstacle, $\alpha_h = 0.49$, for two different tube widths (see legend of Figure 6). Dashed lines represent the limit above which oscillations disappear.

from a symmetric bubble. The oscillations are robust and observed over a wide range of flow rates, tube geometries, and obstacle heights.

The physical mechanism underlying the oscillations must be due entirely to the local change in height of the tube's cross section because oscillations are never observed in uniform rectangular tubes. In any confined, steadily propagating, air-oil displacement flow, the air pressure in the finger is approximately constant and the finger width increases behind the tip because the interface curvature decreases in response to the increase in fluid pressure that drives the axial flow.[16] In the present geometry, when one edge of the finger is located over the obstacle, its curvature within the cross section is constrained. At a critical distance $L_{\rm tip}$ behind the tip, the edge of the widening finger passes sideways over the edge of the obstacle, and there is a dramatic decrease in cross-sectional curvature as the interface expands into the unoccluded region. The induced local increase in pressure drives the oil away from the expanding interface (or bulge), which rapidly moves further sideways until constrained by the tube wall. The system then reaches a quasi-equilibrium state, in which there is a very slow drainage of the thin films of oil adjacent to the tube walls over a much longer timescale than our experiments. The interface in the quasi-equilibrium configuration would have constant mean interface curvature in the absence of gravity, but here the curvature must vary with tube height so that the surface tension can balance the hydrostatic pressure load. In order to maintain an approximately constant mean curvature, however, any change in curvature within the cross section must induce a change in axial curvature. If the change in cross-sectional curvature is set only by the geometry of the tube, the change in axial curvature will be the same for all flow rates, as observed in Figures 3(b)–3(d). Measurements from the images confirm that the axial curvature ratio $r_2/r_1 = 1.86 \pm 0.04$, see Fig. 3(c), in each strongly curved transition region is within 5% of the ratio of the tube height to the height above the obstacle $H/(H-h) = 1/(1-\alpha_h) = 1.96$, consistent with cross-sectional curvature being inversely proportional to the local tube height. Based on these considerations, we believe that the development of a spatially periodic pattern requires the interface to expand over the edge of the obstacle, which only occurs for asymmetric fingers because in the symmetric case the lateral edges of the interface are always within the unoccluded regions.

As Ca increases, the finger broadens more slowly across the obstacle because the increased viscous pressure drop, relative to the capillary pressure scale, induces a more rapid change in curvature, a well-known feature of confined air-oil displacement flows.[16] Hence, $L_{\rm tip}$ increases with increasing Ca, see Fig. 4(a). Consequently, the axial pressure gradient at the point where the interface expands over the obstacle decreases as Ca increases, whereas the local pressure perturbation due to the reduction in mean curvature of the interface as it passes over the edge of the obstacle remains the same on the capillary scale. Hence, as Ca increases, the oil will be evacuated more rapidly from the unoccluded region once the interface has passed over the edge of the obstacle, which in turn

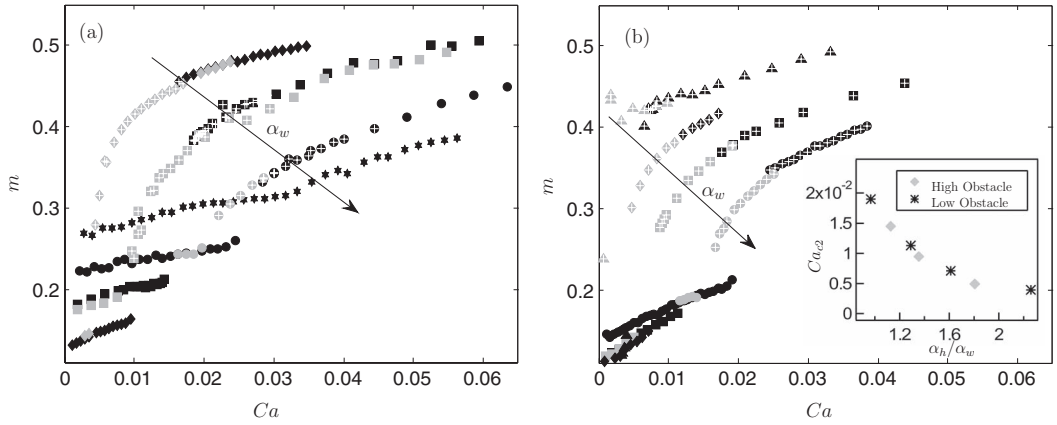

FIG. 5. Wet fraction m as a function of the capillary number Ca. Black markers: Experiments starting from rest; grey markers: experiments starting at a high flow rate that is then reduced. Markers with a white cross correspond to an oscillatory state (a) $\alpha_h = 0.49$: ★ $\alpha_w = 4/7$, ● $\alpha_w = 1/2$, ■ $\alpha_w = 2/5$, ♦ $\alpha_w = 1/3$; (b) $\alpha_h = 0.35$: ● $\alpha_w = 1/3$, ■ $\alpha_w = 1/4$, ♦ $\alpha_w = 1/5$, ▲ $\alpha_w = 1/7$. Inset: Critical capillary number Ca_{c2} above which the symmetric state becomes unstable as a function of the geometric parameter $\alpha_h/\alpha_w = (h/H)/(w/W)$.

causes a more rapid displacement of the interface back over the obstacle on either side of the bulge. This explains why the spatial period of the oscillations decreases as Ca increases. Ultimately, at high enough flow rates, corresponding to the case shown in Fig. 3(e), the large initial tip curvature and rapid adjustment are sufficient to prevent the finger from ever lying over the obstacle and the oscillations cease.

For all oscillatory bubbles, the velocity of the finger tip remains constant within 2% and a timescale $T_{\text{tip}} = L_{\text{tip}}/U$ characterizes the development of the oscillations, see Fig. 4(b). A critical slowing down develops as Ca_{c1}, the capillary number below which oscillations are never observed, is approached from above. Critical slowing down is also in evidence as the capillary number above which oscillations cease, Ca_H, is approached from below, suggesting the presence of another critical point that we conjecture to be a Hopf bifurcation.

For a lower obstacle, $\alpha_h = 0.35$, the fundamental mechanism remains the same, but the cross-sectional curvature above the obstacle is no longer set entirely by the geometry owing to the greater hydrostatic pressure drop above the obstacle. In this case, for sufficiently wide tubes and fast flows, the axial curvature required for an equilibrium configuration can be achieved before the lateral tube wall is encountered and the lateral interface deformations are approximately circular arcs, see Fig. 1.

The global behavior of the system under variations in flow rate and geometry is characterized in Fig. 5, which shows the wet fraction as a function of Ca for $\alpha_h = 0.35$, 0.49, and a number of values of α_w. The wet fraction is calculated using the volume of fluid extracted from the system over a fixed distance and so represents an integrated measure of the spatially periodic finger. In general, m increases with Ca and, for sufficiently wide tubes, above a critical value $Ca_{c2} > Ca_{c1}$ there is an abrupt change that corresponds to the previously observed symmetry breaking,[14] and is usually accompanied by the development of oscillations behind the tip. We note that in that previous work,[14] the finger shapes were characterized by their morphology near the tip, and for the parameter regimes studied, L_{tip} was sufficiently long that the oscillations were not observed. The system exhibits hysteresis and the oscillatory finger states were observed for values below Ca_{c2} by initially withdrawing the fluid at high Ca where oscillations are observed, and rapidly reducing the flow rate. Thus, there are regions of bistability of the symmetric and oscillatory states that occupy a larger range of Ca as α_w decreases, i.e. the tube gets wider relative to the obstacle. For the higher obstacle (Figure 5(a)), the oscillations cease at large enough Ca ($Ca > Ca_H$), which we anticipate will also be the case for the lower obstacle (Fig. 5(b)), but we were unable to achieve sufficiently high Ca experimentally. As α_w increases, the obstacle occupies a greater proportion of the tube width, and the difference in wet fraction between symmetric and oscillatory solutions decreases. The solutions

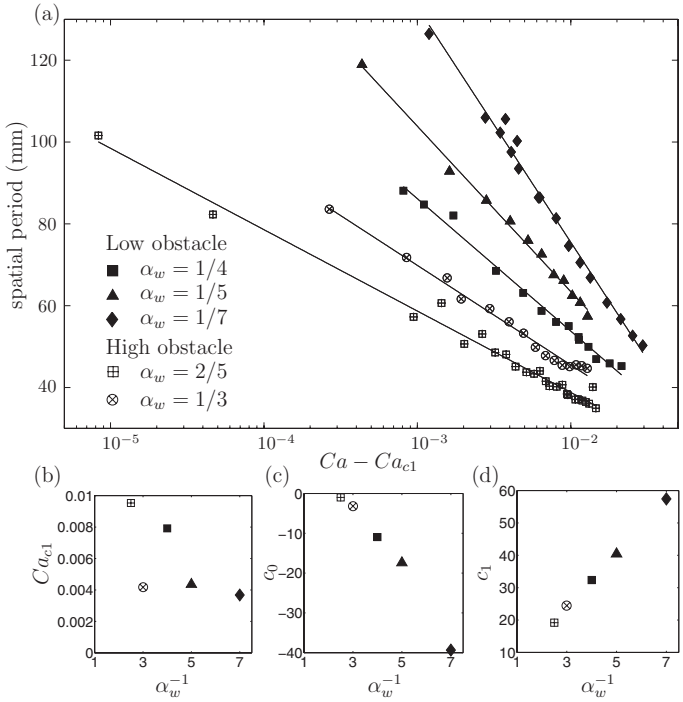

FIG. 6. (a) Spatial period of the oscillations λ as a function of $Ca - Ca_{c1}$, where Ca_{c1} is a critical capillary number above which oscillations appear and is a fitting parameter. Different markers for different obstacles and tube widths α_w; lines are logarithmic fits $\lambda = c_0 - c_1 \log(Ca - Ca_{c1})$. The variation of the fitted parameters with α_w are also shown: (b) Ca_{c1}; (c) c_0; (d) evolution of c_1.

eventually reconnect, before $\alpha_w = 4/7$ when $\alpha_h = 0.49$, and oscillations are no longer observed. The inset in Fig. 5(b) demonstrates that Ca_{c2}, the location of the lateral symmetry breaking, appears to be a function only of a combined geometric factor α_h/α_w, the aspect ratio of the tube divided by the aspect ratio of the obstacle.

Fig. 6 quantifies the dependence of the oscillations on Ca by plotting the spatial period, λ, the dimensional length of a complete waveform, against shifted capillary number, $Ca - Ca_{c1}$, determined via the logarithmic fit $\lambda = c_0 - c_1 \log(Ca - Ca_{c1})$. The spatial period diverges logarithmically at Ca_{c1}, which is indicative of a homoclinic bifurcation.[17,18] The critical capillary number Ca_{c1} decreases with the width of the tube (Fig. 6(b)), but unlike Ca_{c2}, we could not find a straightforward dependence

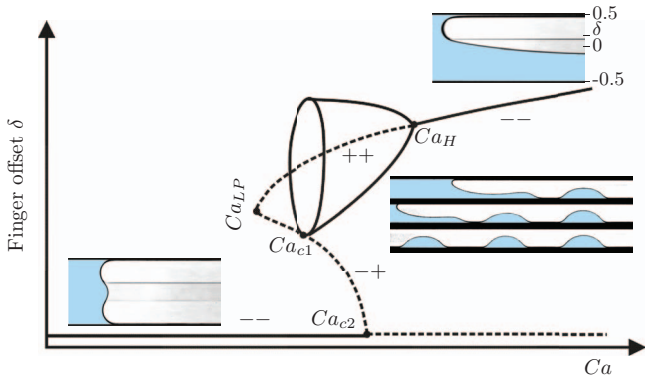

FIG. 7. (Color online) Bifurcation scenario (half shown) in terms of the distance of the finger offset, δ (the location of the mid-width of the finger at a fixed distance behind the tip, relative to tube's centreline). Typical interface shapes corresponding to each of the stable (experimentally observed) solutions are also shown. The signs associated with each steady branch correspond to the signs of the real part of the two leading eigenvalues.

on any geometric parameter. Nonetheless, for each obstacle, Ca_{c1} decreases monotonically with decreasing α_w. In contrast, the other fitted parameters c_0 and c_1 are approximately linear functions of α_w^{-1}, consistent with the fact that similar lateral broadening (at an approximately constant rate) of the finger in response to the change in cross-sectional curvature is the physical mechanism underlying the oscillations for both obstacle heights.

A bifurcation structure consistent with the experimental evidence is shown Fig. 7. Symmetry is lost via a subcritical pitchfork bifurcation at Ca_{c2} and the unstable asymmetric solution branch is further destabilized through a limit point at $Ca_{LP} < Ca_{c2}$. At $Ca_H > Ca_{c2}$, the asymmetric solution is restabilized through a supercritical Hopf bifurcation and a stable periodic orbit exists for $Ca < Ca_H$. In a frame moving with constant speed of the finger tip, the Hopf bifurcation is a temporal bifurcation at a fixed location relative to the finger tip. The resulting oscillatory solutions are those observed in our experiments and they disappear at Ca_{c1} via a homoclinic connection between the unstable and stable manifolds of the unstable asymmetric solution in the region (Ca_{LP}, Ca_{c2}). The disappearance of the oscillations and reconnection of the solutions can be achieved by a variety of codimension-two scenarios that we have not attempted to determine experimentally.

In conclusion, the dynamics of displacement-driven fluid extraction from axially uniform pores with locally constricted cross sections can be completely different from the simple behavior found in idealized geometries, which suggests that in certain flow regimes the predictive power of models based on idealized geometries is severely compromised. Moreover, we have also found that finite bubbles driven by constant flux can oscillate, resulting in the periodic deformation of the entire bubble. This offers further potential for geometry-induced manipulation of droplets for lab-on-the-chip applications, and a detailed study is currently underway.

The support of EPSRC is gratefully acknowledged (Grants EP/H011579/1 and GR/S99402/01).

[1] M. Sahimi, "Flow phenomena in rocks: From continuum models to fractals, percolation, cellular automata, and simulated annealing," Rev. Mod. Phys. **65**, 1393 (1993).
[2] G. M. Whitesides, "The origins and future of microfluidics," Nature **442**, 368 (2006).
[3] J. B. Grotberg and O. E. Jensen, "Biofluid mechanics of flexible tubes," Annu. Rev. Fluid Mech. **36**, 121 (2004).
[4] G. I. Taylor, "Deposition of viscous fluid on the wall of a tube," J. Fluid Mech. **10**, 161 (1961).
[5] A. de Lózar, A. Juel, and A. L. Hazel, "The steady propagation of an air finger into a rectangular tube," J. Fluid Mech. **614**, 173 (2008).
[6] C. Clanet, P. Hérault, and G. Searby, "On the motion of bubbles in vertical tubes of arbitrary cross-sections: some complements to the Dumitrescu–Taylor problem," J. Fluid Mech. **519**, 359 (2004).
[7] H. Wong, C. J. Radke, and S. Morris, "The motion of long bubbles in polygonal capillaries. Part 1. Thin films," J. Fluid Mech. **292**, 71 (1995).
[8] C. Hollis, V. Vahrenkamp, S. Tull, A. Mookerjee, C. Taberner, and Y. Huang, "Pore system characterisation in heterogeneous carbonates: an alternative approach to widely used rock-typing methodologies," Mar. Pet. Geol. **27**, 772 (2010).
[9] M. Heil, A. L. Hazel, and J. A. Smith, "The mechanics of airway closure," Respir. Physiol. Neurbiol. **163**, 214 (2008).
[10] H. A. Stone, A. D. Stroock, and A. Adjari, "Engineering flows in small devices," Annu. Rev. Fluid Mech. **36**, 381 (2004).
[11] C. N. Baroud, F. Gallaire, and R. Dangla, "Dynamics of microfluidic droplets," Lab Chip **10**, 2032 (2010).
[12] H. Gu, M. H. G. Duits, and F. Mugele, "Droplets formation and merging in two-phase flow microfluidics," Int. J. Mol. Sci. **12**, 2572 (2011).
[13] M. Fermigier, L. Limat, J. E. Wesfreid, P. Boudinet, and C. Quilliet, "Two-dimensional patterns in Rayleigh–Taylor instability in a thin layer," J. Fluid Mech. **236**, 349 (1992).
[14] A. de Lózar, A. Heap, F. Box, A. L. Hazel, and A. Juel, "Partially-occluded tubes can force switch-like transitions in the behavior of propagating bubbles," Phys. Fluids **21**, 101702 (2009).
[15] A. de Lózar, A. L. Hazel, and A. Juel, "Scaling properties of coating flows in rectangular channels," Phys. Rev. Lett. **99**, 234501 (2007).
[16] A. L. Hazel and M. Heil, "The steady propagation of a semi-infinite a semi-infinite bubble into a tube of elliptical or rectangular cross-section," J. Fluid Mech. **470**, 91 (2002).
[17] P. Gaspard, "Measurement of the instability rate of a far-from-equilibrium steady state at an infinite period bifurcation," J. Phys. Chem. **94**(1), 1 (1990).
[18] A. J. Homburg and B. Sandstede, "Homoclinic and heteroclinic bifurcations in vector fields," in *Handbook of Dynamical Systems* (North-Holland, Amsterdam, 2010), Vol. 3, pp. 379–524.
[19] See supplementary material at http://dx.doi.org/10.1063/1.3682772 for movies of the temporal development of the spatially periodic pattern. The steadily advancing finger "sheds" a spatially-periodic pattern, through the local sideways oscillatory motion of the interface at a fixed distance behind the bubble tip for $\alpha_w = 1/5$ and $\alpha_h = 0.35$: (a) $\mathrm{Ca} = 6.0 \times 10^{-3}$ (6.7 × real time); (b) $\mathrm{Ca} = 1.59 \times 10^{-2}$ (6.6 × real time).